Diagnosing cross-scale kinetic energy exchanges from two submesoscale permitting ocean models.

A. O. Ajayi[1], **J. Le Sommer**[1], **E. Chassignet**[2], **JM. Molines**[1], **X. Xu**[2], **A. Albert**[1], and **W. Dewar**[2]

[1]Universite Grenoble Alpes /CNRS/IGE, Grenoble, France.
[2]Florida State University, Tallahassee, USA.

This is a non-peer reviewed preprint submitted to ESSOAr.
This manuscript has been submitted on the 16th of October 2019, to the Journal of Advances in Modeling Earth Systems.

Abstract

The upper-ocean at fine-scales (<100 km) contributes significantly to energy exchanges and dissipation. However, our knowledge of fine-scale motions (in terms of kinetic energy density and transfer) in the real ocean is limited due to lack of sufficient observational datasets at these scales. Kilometric resolving ocean models have been developed in anticipation for the Surface Water and Ocean Topography (SWOT) satellite mission. This mission would provide unprecedented global coverage of energetic oceanic flows down to 10 km. In this study, we investigate the distribution and exchange of energy across different scales down to 10 km based on two state-of-the-art realistic North Atlantic basin simulations with horizontal resolution of ~ 1.5 km. The results show that ageostrophic motions have direct impacts on cross-scale kinetic energy exchanges and that these exchanges undergo both regional and seasonal variability. In particular, this seasonality which is more pronounced at fine-scale is characterized by a significant amount of direct KE cascade in wintertime. In general, we found the forward cascade to be confined to the mixed layer depth while the inverse cascade extends down to about 700m in the interior.

1 Introduction

The world ocean is a turbulent fluid with a very broad range of energetic scales, ranging from large $\sim$O(1000km) to centimeter scales. The ocean kinetic energy is mostly

concentrated in quasi-geostrophic mesoscale eddy field with scales $\sim$O(100 km) (Stammer and Böning, 1992). Due to non-linear interactions among different length scales, energy can be transferred both from large to small (forward, or direct cascade) and from small to large scale (inverse cascade). Understanding the distribution of kinetic energy and variance across scale in oceanic flows is, therefore, key to our knowledge of ocean circulation (Ferrari and Wunsch, 2009).

To estimate the variance and energy associated with eddy motions at different scales, velocity wavenumber spectral density has proven to be very efficient (Le Traon et al., 1990, 2008; Fu et al., 2010; Dufau et al., 2016; Uchida et al., 2017). However, spectral density does not indicate the direction of kinetic energy exchanges between the different scales. A better knowledge of cross-scale energy exchanges is gained by looking at the KE cascade due to nonlinearity. This important feature in turbulence study dates back to the work of Charney (1971) and Salmon (1980) on geostrophic turbulence. For stratified rotating quasi-two-dimensional fluid motion, classical geostrophic turbulence theory predicts a direct cascade of energy if the flow is depth-dependent (baroclinic) but an inverse cascade of energy if the flow is depth-independent (barotropic). In particular, for the ocean with a surface intensified stratification, energy from higher baroclinic modes concentrates in the first mode and then undergoes a direct cascade towards the deformation scale (R_d) (Smith and Vallis, 2002). At R_d, baroclinic energy is converted to barotropic mode via barotropization. At this point, most of the energy near the deformation scale cascade towards larger scale while a small fraction undergoes direct cascade to dissipation (see Figure 1).

This prediction of geostrophic turbulence theory has been observed both in the virtual ocean and the real ocean but with a little discrepancy. Based on altimeter data, Scott and Wang (2005) showed that the (Pacific) ocean is dominated by an inverse cascade of energy at scales larger than R_d. So, if one agrees that the altimeter data is reflecting the first baroclinic mode (Smith and Vallis, 2002), then this is in contrast with geostrophic turbulence theory which predicts a forward cascade for a baroclinic flow. From this discrepancy, two questions arise. (i) is the inverse cascade seen at the surface due to the barotropic mode? or (ii) is it possible that the baroclinic modes experience an inverse cascade? Scott and Arbic (2007) using a 2-layer model simulation showed that the inverse cascade at the ocean surface is mostly baroclinic with a small contribution from the barotropic mode. More recent literature Eden (2007); Sasaki et al. (2017); Tulloch et al. (2011); Aluie et al. (2017); Brüggemann and Eden (2015); Kjellsson and Zanna (2017); Khatri et al. (2018) have also shown that inverse cascade of energy mostly dominates the surface ocean at scales larger than R_d.

Indeed we know much about the inverse-cascade-dominated-ocean-surface for scales larger than the deformation radius. What about at fine-scales where ocean struc-

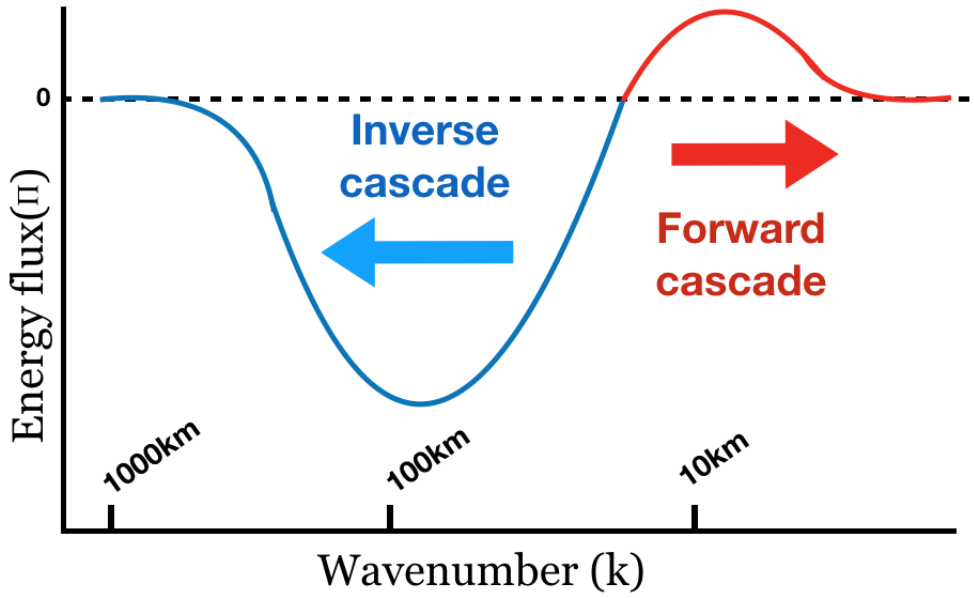

Figure 1: Schematics of kinetic energy spectral flux. Blue : inverse cascade of energy, Red : forward cascade of energy.

tures are very energetic and are highly modulated seasonally? In fact, at scales < 100 km, oceanic motion includes energetic submesoscale motions (< 50km). Results from numerical simulation and observation have shown an injection of energy in wintertime at submesocales (Sasaki et al., 2017). This energy injection is partly responsible for both meso and submesoscale seasonality (Uchida et al., 2017; Capet et al., 2008a; Sasaki et al., 2014) and has been argued to be associated with mixed layer instability (Callies et al., 2015; Qiu et al., 2014; Sasaki et al., 2014; Brannigan et al., 2015; Rocha et al., 2016). This seasonality is responsible for the shallowing of KE spectra slope from -3 in summer to -2 in winter. This is usually interpreted as a shift from a turbulence dominated by interior gradients (Charney regime) to a regime dominated by surface driven turbulence (Philips regime) (Sasaki et al., 2014). Apart from the work of Sasaki et al. (2017, 2014), we are unaware of any investigation on the implication of submesoscale seasonality on cross-scale energy exchanges at basin scale. There are also a few other open questions with regard to energy transfer at fine-scales that are worth investigating, e.g., (i) what are the range of scales that corresponds to forward and inverse cascade of energy, (ii) the depth penetration of this cascade and in particular (iii) how much energy is cascaded in the forward direction at fine scale.

Submesoscale resolving ocean models have been developed in anticipation for the Surface Water and Ocean Topography (SWOT) satellite mission (Fu et al., 2010). At a global scale, satellite altimeter remains the major source of information on the distribution of energy across scales. However, at the moment, the resolution capability of our existing ocean-observing satellite altimeter stands at roughly 70 km

(Dufau et al., 2016). This limitation undermines our ability to investigate energy exchanges at scales < 100 km. To solve this challenge, SWOT is been implemented to provide 10 times higher resolution than conventional altimeters and numerical ocean models have been designed to prepare for SWOT. These state-of-the-art numerical experiments with high resolution capability thereby provide an opportunity to study cross-scale energy exchanges down to kilometric scales while keeping in mind the aforementioned open questions.

To this end, the aim of this study is to investigate the distribution and transfer of energy across different scales by using outputs of two sub-mesoscale permitting ocean models of the North Atlantic. In particular, we focus on the seasonality and depth penetration of cross-scale KE variance and transfer with an emphasis on scales < 100 km. This paper is organized as follows, section 2 presents a short description of the two numerical simulations. In section 3, we examine the kinetic energy wavenumber spectral density and slope. The KE cascade, the seasonality and the influence of ageostrophic flow on energy cascade in the North Atlantic are discussed in section 4. Finally, in section 5 we summarize the findings and discuss the relevance of this work to the anticipated SWOT mission.

2 North Atlantic Numerical Simulations

In this study, we use numerical outputs from two submesoscale eddy-permitting simulations of the North Atlantic: a NEMO-based simulation with a horizontal resolution of 1/60° (NATL60) and a HYCOM-based (HYbrid Coordinate Ocean Model) simulation with a horizontal resolution of 1/50° (HYCOM50).

The NEMO-based NATL60 has a horizontal grid spacing ranging from 1.6 km at 26°N to 0.9 km at 65°N. The initial and open boundary conditions are based on the GLORYS2v3 ocean reanalysis with a relaxation zone at the northern boundary for sea-ice concentration and thickness. The model has 300 vertical levels with a resolution of 1 m at the top-most layers. The atmospheric forcing is based on DFS5.2 Dussin et al. (2018) and the grid and bathymetry follows Ducousso et al. (2017). In order to implicitly adapt lateral viscosity and diffusivity to flow properties, a third-order upwind advection scheme is used for both momentum and tracers in the model simulation. The model is spin-up for a period of six months, and a one-year simulation outputs from the year 2012 to 2013 are used in this study. A description of the NATL60 simulation is available from Le Sommer et al. (2019) and the outputs have been used in the recent studies by Fresnay et al. (2018) and Amores et al. (2018).

The HYCOM-based HYCOM50 extends from 28°S to 80°N and has a horizontal

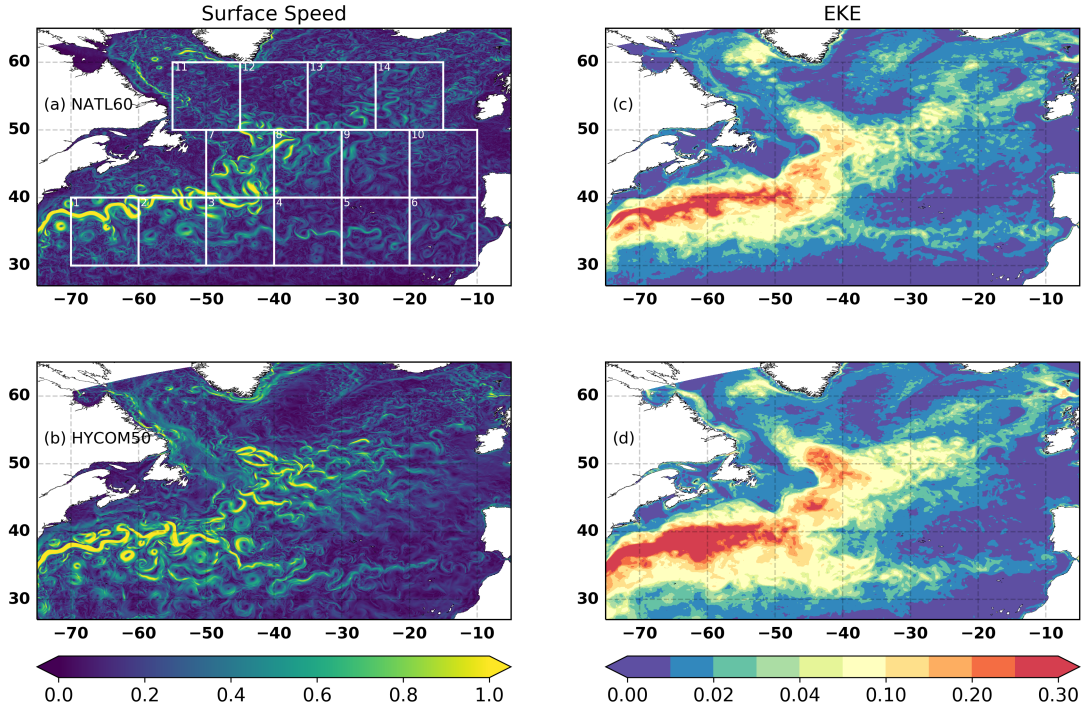

Figure 2: Left panel : snapshot of surface speed on march 1st for NATL60 and HYCOM50. Right panel : eddy kinetic energy computed from daily output of surface velocity field.

grid spacing ranging from 2.25 km at the equator, $\sim$1.5 km in the Gulf Stream region, and 1 km in the subpolar gyre. As for NATL60, the effective resolution is about 10–15 km. The vertical coordinate is hybrid and consists of 32 layers. The simulation is initialized using potential temperature and salinity from the GDEM climatology and spun up from rest for 20 years using climatological atmospheric forcing from ERA-40 (Uppala et al., 2005), with 3-hourly wind anomalies from the Fleet Numerical Meteorology and Oceanography Center 3-hourly Navy Operational Global Atmospheric Prediction System (NOGAPS) for the year 2003. The year 2003 is considered to be a neutral year over the 1993 to present timeframe in terms of long-term atmospheric patterns of the North Atlantic Oscillation. The last year of the simulation is used to perform the analysis. The horizontal viscosity operator is a combination of Laplacian and Biharmonic. The bathymetry is based on the Naval Research Laboratory (NRL) digital bathymetry database. The model configuration and a detailed evaluation of the model results in the Gulf Stream region with observations are documented in Chassignet and Xu (2017).

Both NATL60 and HYCOM50 resolve the first Rossby radius of deformation everywhere within the model domains and these simulations reproduce realistic eddy statistics with levels of kinetic energy in the range of altimetric observations (Le Sommer et al., 2019; Chassignet and Xu, 2017) (Figure 2). HYCOM50 shows a higher eddy kinetic energy (EKE) level along and around the Gulf Stream-North

Atlantic Current path. The less energetic Gulf Stream-North Atlantic Current in the NATL60 simulation may be due, in part, to its shorter spin-up period (6 months versus 19 years). A summary of the model parameters is tabulated in Table 1.

Table 1: Table of model parameters for NATL60 and HYCOM50

	NATL60	HYCOM50
Domain	26.5N - 65N	28 - 80N
Numerical Code	Nemo v.3.6	HYCOM
Horizontal grid	1/60: 0.9-1.6 km	1/50:1.1-2.2 km
Vertical coordinate	Z partial cells	Hybrid (Z & isopycnal)
Vertical grid	300 Levels : 1-50 m	32 Layers
Boundary conditions	GLORYS2v3	GDEM
Atmospheric forcing	DFS5.2	ERA-40
Horizontal Viscosity	Implicit in momentum advection	Laplacian & Biharmonic

Since the NATL60 covers a smaller domain than HYCOM50, we consider the HYCOM50 outputs for exactly the same region covered by NATL60 to have comparable results and we perform spectral analysis in sub-domains of 14 $10^\circ \times 10^\circ$ boxes across the North Atlantic. We focus specifically on quantifying kinetic energy wavenumber spectral density (Eq. 1) and flux (Eq. 2) using horizontal velocity fields. In equation (1) and equation (2),$\hat{}$refers to Fourier transform, * represents the complex conjugate, Re refers to the real part of a complex number and $k = \sqrt{k_x^2 + k_y^2}$. Before performing spectral analysis the 2D velocity field from each subdomain (box) is detrended in both direction and a 50% cosine taper window (turkey windowing) is applied for tapering. An FFT is applied to the tapered data and a 1D isotropic spectrum is obtained by averaging in the azimuthal direction. Our spectra method is consistent with procedures previously used in Stammer and Böning (1992); Sasaki and Klein (2012); and Chassignet and Xu (2017).

$$E(k) = \int_k^{k+\delta k} \left[\widehat{\mathbf{u}}^* \cdot \widehat{\mathbf{u}}\right](k)dk \tag{1}$$

$$\Pi(k) = \int_k^{k_s} -Re\left[\widehat{\mathbf{u}}^* \cdot \left(\widehat{\mathbf{u} \cdot \nabla_{\mathbf{H}}\mathbf{u}}\right)\right](k)dk \tag{2}$$

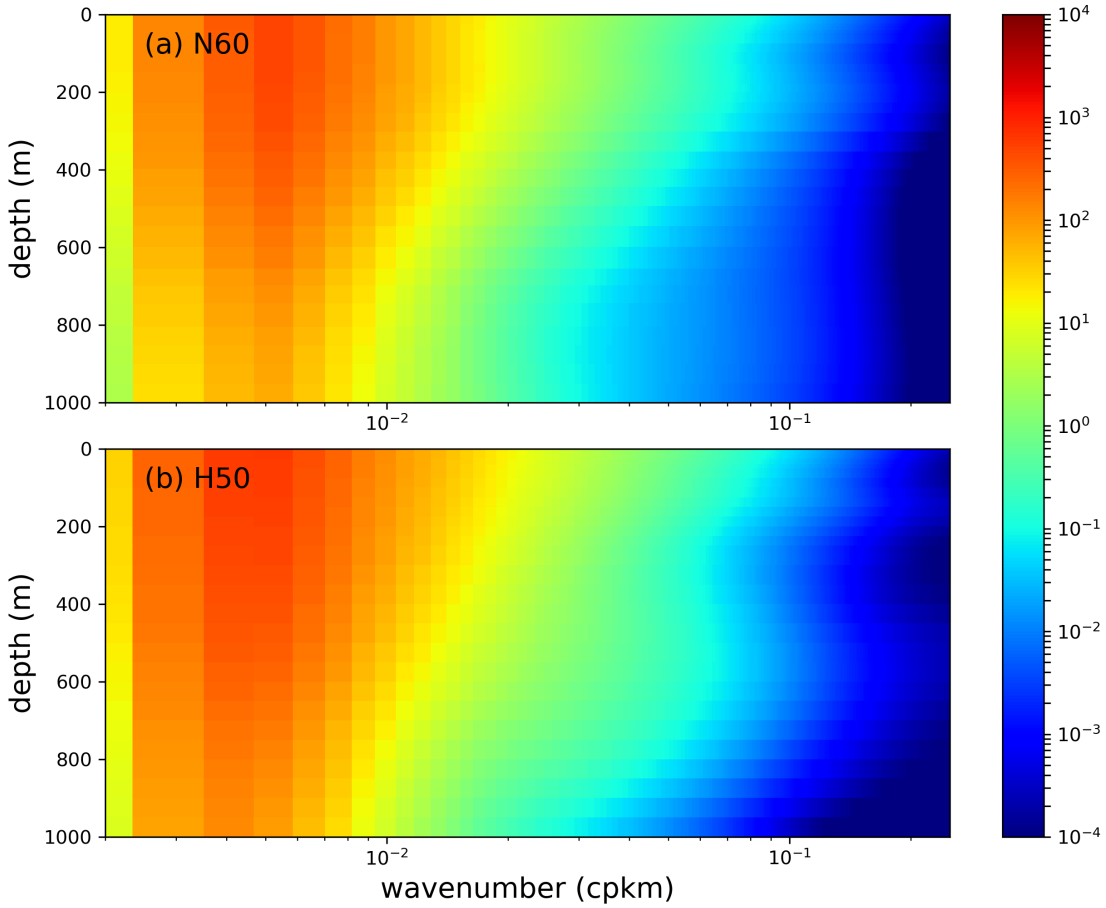

Figure 3: One year average of kinetic energy spectral density (computed from daily outputs for Box 8) as a function of depth for (a) NATL60 and (b) HYCOM50.

3 Distribution of Kinetic Energy

3.1 Spectral Density

We present in this section the analysis of the kinetic energy wavenumber spectra as a proxy to quantify the energy across different scales of motions. In Figure 3 we present the KE spectral density as a function of depth for the two simulations (Box 8). The peak of the spectral density is around the mesoscale motions (100–500 km) and, as expected, the energy associated with large scale motion are relatively higher compared to that of fine-scales. The peak is preserved with depth, but the variance at all scales decreases with depth. The decrease in the spectral variance with depth relative to the surface is more pronounced at the fine scales when compared to large scales. This indicates that the fine-scale structures (relative to the surface) are less energetic in the interior of the ocean.

The comparison between the two simulations is better illustrated in Figure 5a where

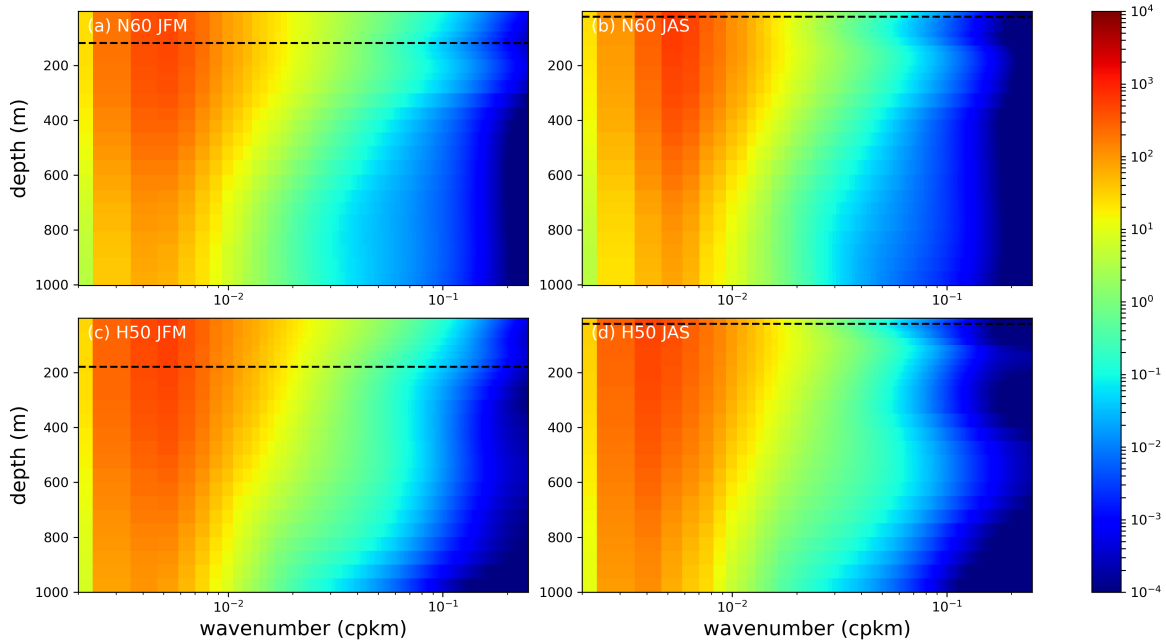

Figure 4: Winter and summer averages of kinetic energy spectral density for Box 8 computed from horizontal total velocity as a function of depth for (a) NATL60 and (b) HYCOM50.

we present the annual, winter and summer depth-averages of KE spectra density for the two simulations in the same region (Box 8). The spectral density from the two models agrees well and both are consistent with the QG prediction with a spectral shape of k^{-3}. There is a strong seasonality in the variance associated with fine-scale motions (Figure 4 and 5b). The increase in spectral density observed in wintertime at high wavenumbers underscores the energetic nature of fine-scale structures in wintertime. From the KE density plot, we also see that HYCOM50 is more energetic than NATL60 both at the surface and also in the interior.

The disparity between the energy level of the two models is not the main focus of this paper. Having said that, we propose a few reasons why the two model could differ in terms of energetics. Firstly, the eddy structures in NATL60 are not fully developed due to the short spin-up (6 months for NATL60 versus 20 years for HYCOM50). The first 2 years of the HYCOM50 simulation show a clear increase of total kinetic energy level; see Figure 2 in Chassignet and Xu (2017). Furthermore, as recently documented in Ajayi et al. (2019), the typical eddy scales are smaller in NATL60 (than in HYCOM50) and this could be a direct consequence of the shorter spin-up length. Secondly, the question did arise as to whether the coarser vertical resolution in HYCOM50 (32 hybrid vertical layers versus 300 z-levels in NATL60) could lead to a stronger inverse cascade and hence a higher energy level because of an under-resolved stratification and the depth dependence of flows. However, a comparison of the vorticity spectral coherence with respect to depth shows that the two simulations

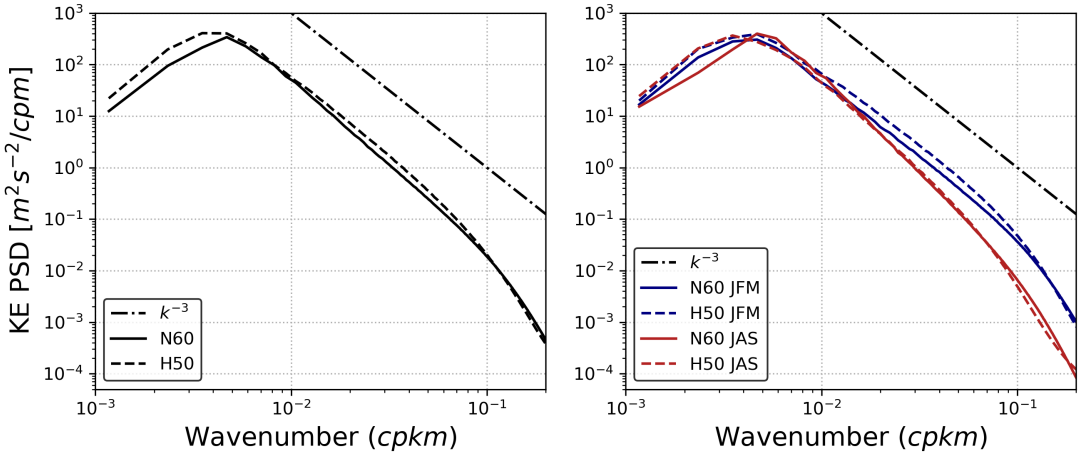

Figure 5: Kinetic energy spectra density for Box 8 (averaged over 1000m depth) computed from daily output of horizontal total velocity for NATL60 (thick line) and HYCOM50 (dash line). (a) one year mean (b) winter (blue line) and summer (red line) averages.

are essentially identical in terms of the depth penetration of energetic eddy structures (Ajayi et al., 2019). Furthermore, in section 4, a comparison of the KE spectral flux at depths for the two simulations will show that the HYCOM50 upscale energy flux is not surfaced intensified and that having only 32 isopycnal vertical levels is not detrimental to the representation of the dynamics in the ocean interior. Thirdly, the choice of sub-grid parameterization is different between the two simulations and could possibly have a strong effect on how energy is dissipated between them.

3.2 Spectral Slope

Horizontal wavenumber spectral density generally exhibits power-law behavior, where the exponent is interpreted in terms of the dynamical processes governing the eddy energy transfer. Existing theoretical frameworks predict (for horizontal velocity) a spectral slope of -3 and -5/3 for Quasigeostrophic (QG) and surface quasi-geostrophic (SQG) turbulence respectively. A slope of -2 is also well known for a front dominated flow (Fu and Ferrari, 2008). Over the years, many research works have tried to establish the accuracy of these predictions by using outputs of realistic ocean models (Sasaki and Klein, 2012; Chassignet and Xu, 2017; Uchida et al., 2017) and also recently within context of the real ocean by using altimeter dataset (Le Traon et al., 1990; Dufau et al., 2016). Their results have argued for the non-existence of a universal wavenumber spectrum (Le Traon et al., 2008) following observed regional variability.

A quick way to estimate the wavenumber spectral power law is to compute the 1D wavenumber spectra then estimate a slope from this spectra by fitting a line to the

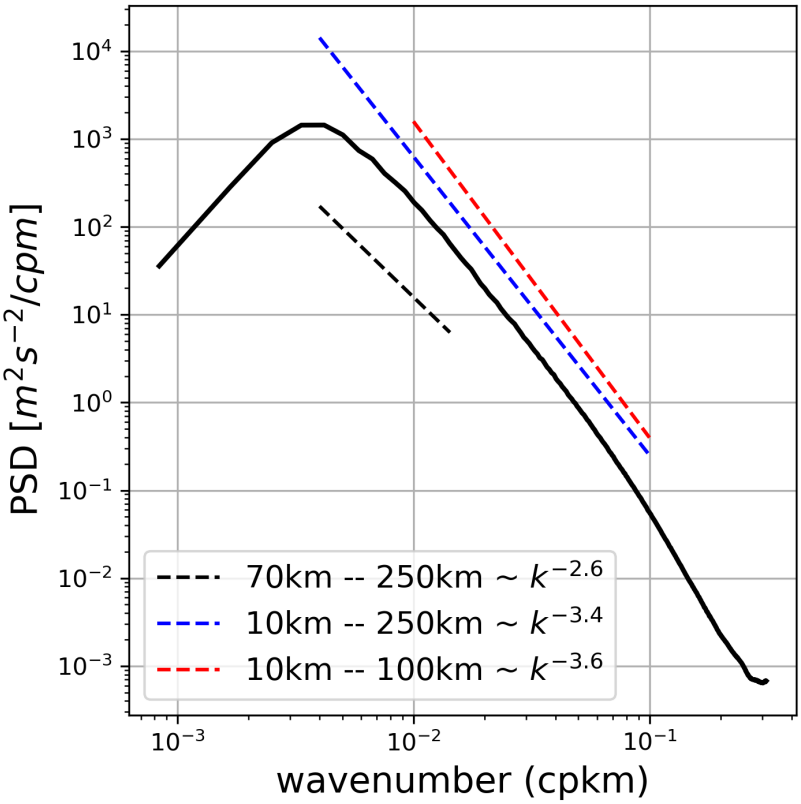

Figure 6: Average KE wavenumber spectral and slope for box 1 in the month of March for three different selected wavenumber range. The wavelengths range are represented by dashed lines with the color red, blue and black for 10-100km, 10-250km and 70 – 250km respectively.

spectral density curve within a selected wavenumber range. This method is fast and easy to implement and provides a way to investigate regional variability of ocean energetics both at the basin and global scale. For studies focused on mesoscale energetics using satellite datasets and model outputs, this wavenumber range is mostly within the error limits of the altimeter ($\sim$ 70 km) with an upper bound of 250–300 km. One drawback of this approach is that it does not account for the changes in the scale of average energetic eddy structures with latitude. Scales of motions that are mesoscales in the polar regions are classified as sub-mesoscales in the tropics.

A number of recent studies have tried to propose different approaches to estimate wavenumber spectral power law as a way to correctly characterize the spectral signature. Oscar et al. (2018) estimated spectra slope for mesoscale motions by computing the slope between the peak of the spectra and the minimum ofthe Rossby radius and the Rhines scale following Eden (2007). A similar approach was presented in Sasaki and Klein (2012), where the authors estimated spectral slope between a fixed wavelength of 30 km (at the lower bound) and the scale that corresponds to the peak of the KE wavenumber spectra.

In order to show how sensitive the estimated slopes are to the selected wavelength range, we present in Figure 6 the average KE wavenumber spectra and slope for box 1 in the month of March for three different selected wavenumber ranges. The wavelengths are represented by dashed lines with the color red, blue and black for 10–100 km, 10–250 km and 70–250 km respectively. The estimated slopes for these three different wavelength range have different values, therefore raising the question as to which slope is most representative of the dynamics of this region. We repeat this analysis for all the boxes and present the map in Figure 7. The mismatch is particularly pronounced at the sub-polar region, where the scales of the eddy structures are smaller. The 70–250 km wavelength range is a typical wavelength for estimating spectral slope for satellite datasets because 70 km roughly corresponds to the wavelength where the satellite data becomes noisy. The spectral slope in this range is fairly consistent with the already published work of Dufau et al. (2016) and Chassignet and Xu (2017).

To avoid the sensitivity of the estimated spectral slope to an a-priori selected wavelength range, we introduce an approach that takes into account the dynamics of the regions and the resolving capability of the model by estimating the spectral slope (Figure 8) between the energy-containing scale (Kjellsson and Zanna, 2017) and the effective resolution of the model (Soufflet et al., 2016). The energy-containing scale (which represents the scale of the most energetic eddy structure) is estimated from the kinetic energy wavenumber spectra using equation (3) while the effective resolution (a function of the model grid-size) is taken as 5 $\times$ the model grid size and this is roughly equally to 10 km for both models. This approach takes into account

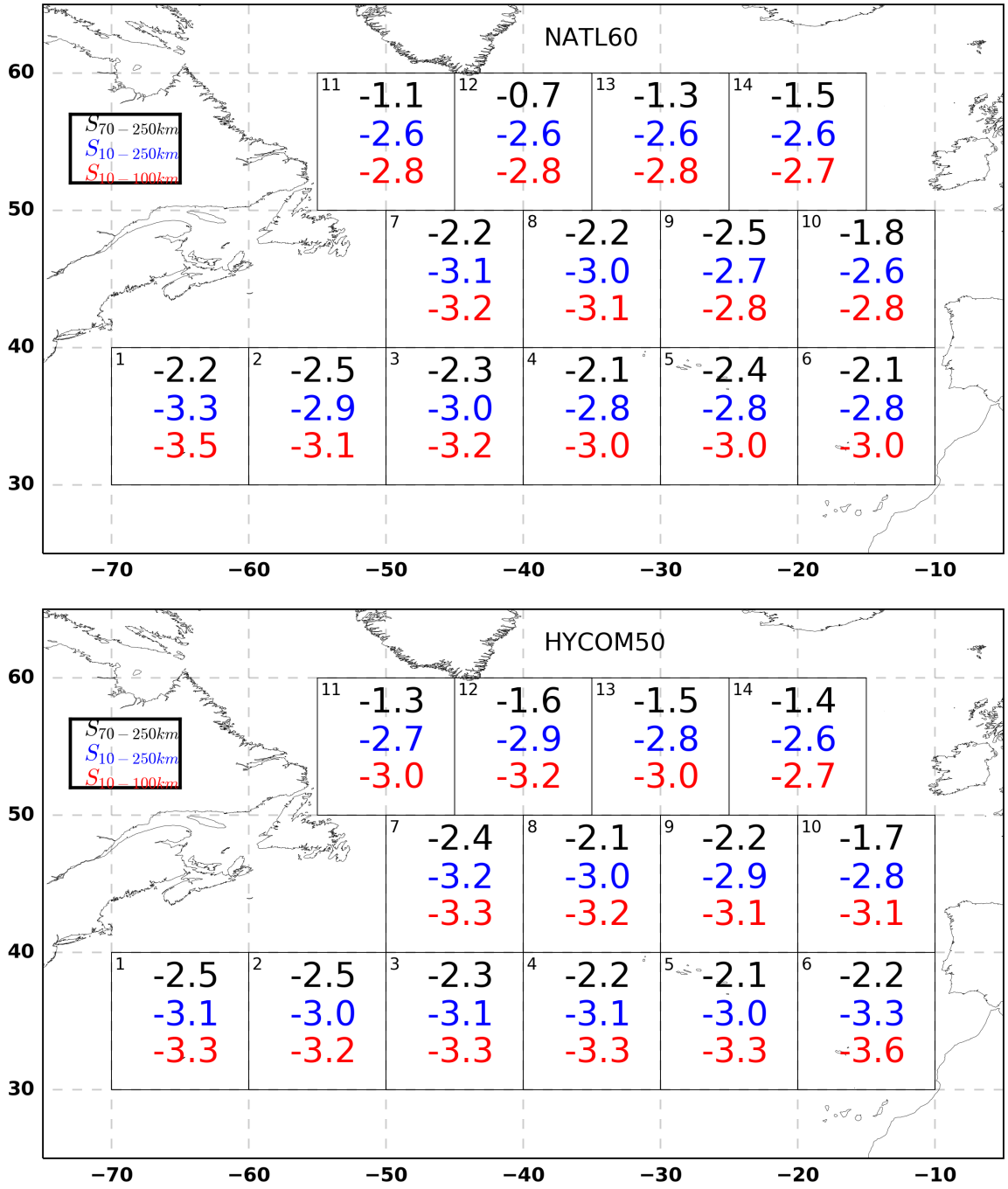

Figure 7: Map of spectral slope estimated from three different wavelength range. Colour red, blue and black represent 10 - 100km , 10 - 250km and 70 - 250km respectively

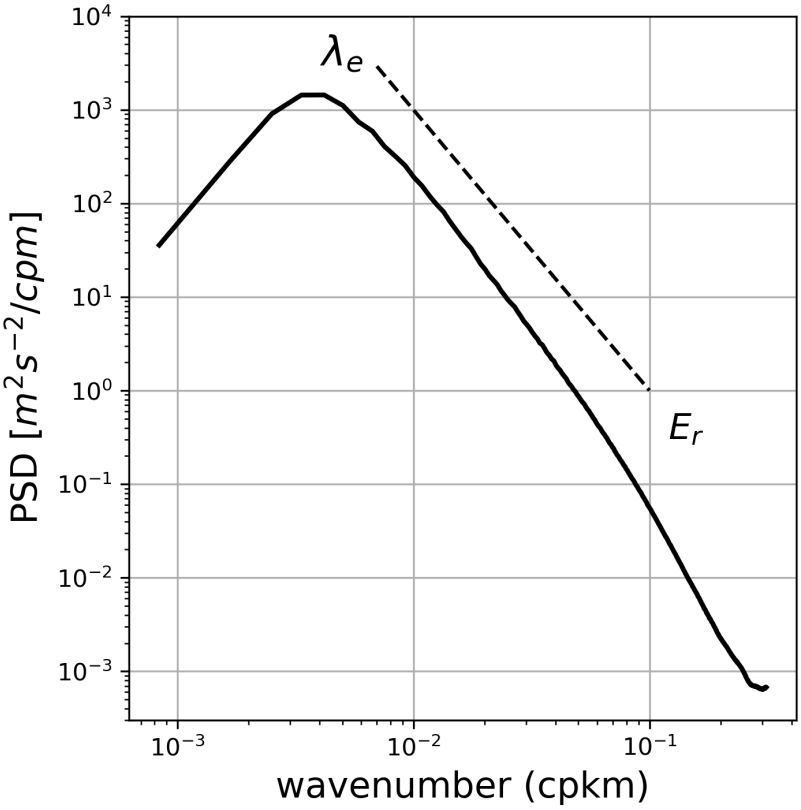

Figure 8: A schematic illustrate the proposed dynamical approach to estimate spectral slope.

the scale of the energetic eddy structures within the flow region and also takes into account the geographical variability of this scale, and therefore provides a way to infer dynamical properties of oceanic motions in different regions.

$$\lambda_e = \frac{\int\int E(k_x, k_y) dk_x dk_y}{\int\int \sqrt{k_x^2 + k_y^2} E(k_x, k_y) dk_x dk_y} \tag{3}$$

We apply this technique to the output of both simulations and we present the estimated spectral slope and the energy-containing scale (integral scale) for all the boxes in the North Atlantic (Figure 9). The estimated integral scale from the wavenumber spectra represents the averaged scale of energetic motions in the selected region. On one hand, this scale varies regional and fairly follows the variability of the Rossby radius of deformation with latitude, with high values in the south and relatively low values in the north. On the other, the estimated slope across the basin is almost uniform and follows the prediction of QG with a slope value $\sim k^{-3}$. This consistency with the QG prediction is observed in both model outputs and also holds in the well known high energetic Gulf stream (box 1) and the low energetic OSMOSIS (box 10) regions. This result suggests that the North Atlantic Ocean is well described by QG dynamics.

4 Kinetic Energy Cascade

In this section, we present and discuss the exchange of energy due to non-linearity across different scales of motion. This exchange is estimated from the horizontal velocity fields using equation (2). A positive flux represents a direct cascade of energy while a negative value represents an inverse cascade of energy. The novelty of the estimated spectral flux presented in this study is partly based on the ability of the models to reasonably resolve the cross-scale energy exchanges at scales $<$100 km.

We show in Figure 10, the result of the KE spectra flux computed using one year daily outputs of surface velocity fields. For simplicity, we show plots for box 3, 8 and 11 representing latitudes of 35N, 45N, and 55N respectively. In all the boxes and in both model outputs, the spectral flux is dominated by an inverse cascade of energy at large scales (between 25-50km and 500km) and a forward cascade of energy below 25-50 km. Depending on the region, part of the submesoscale range of 0 to 50km (as defined by Sasaki et al. (2017)) falls to the left of the zero-crossing (where the flux changes sign). This implies that a significant part of submesoscales motions are involved in fluxing energy to large scales via an inverse cascade of energy, and this, in a way indicates how submesoscales flow impact meso and large scales circulations via energy exchanges.

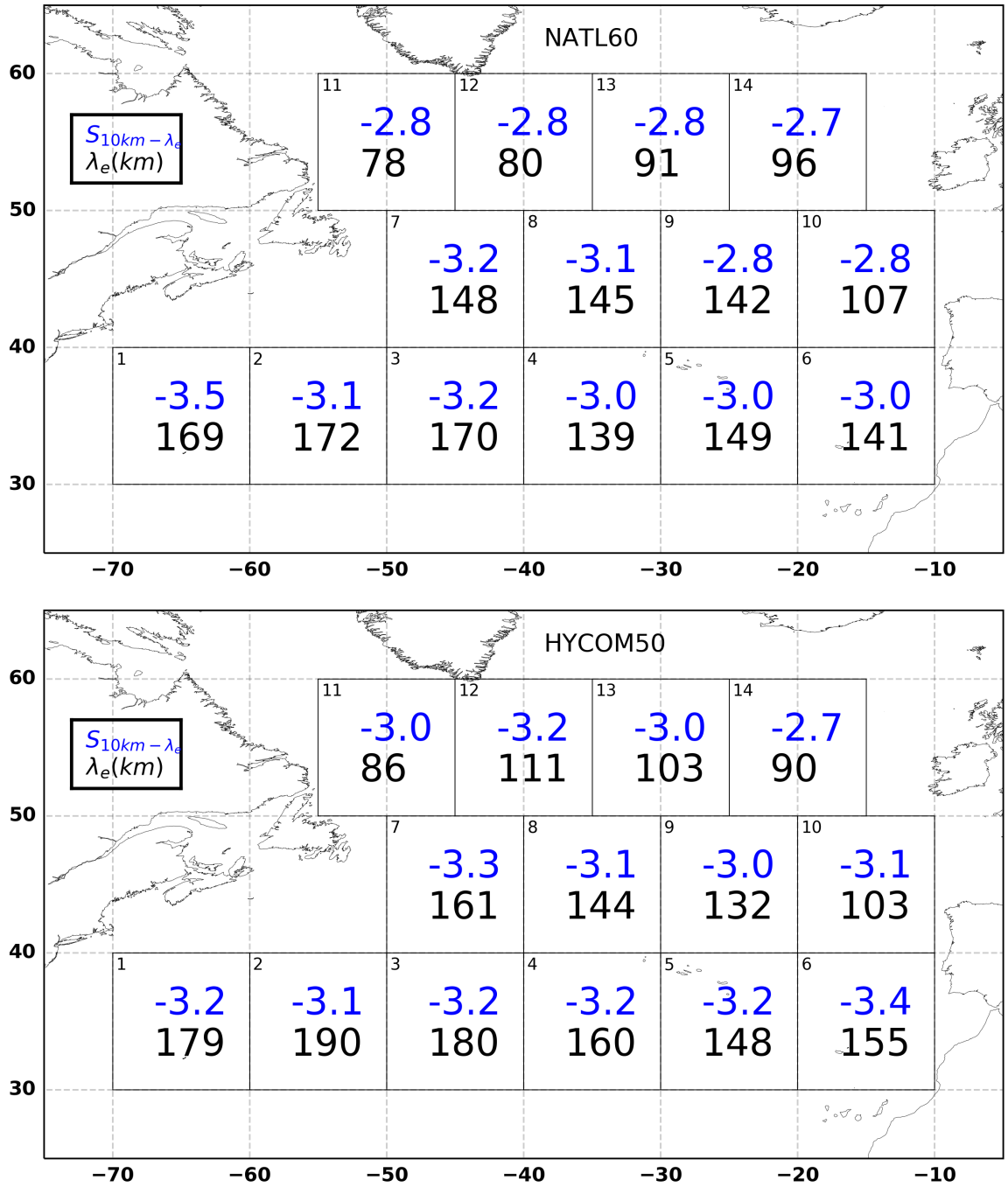

Figure 9: Blue colour : spectral slope estimated between the model effective resolution (E_f) and the integral scale (λ_e). Black colour : energy containing scale estimated from the kinetic energy wavenumber spectral density

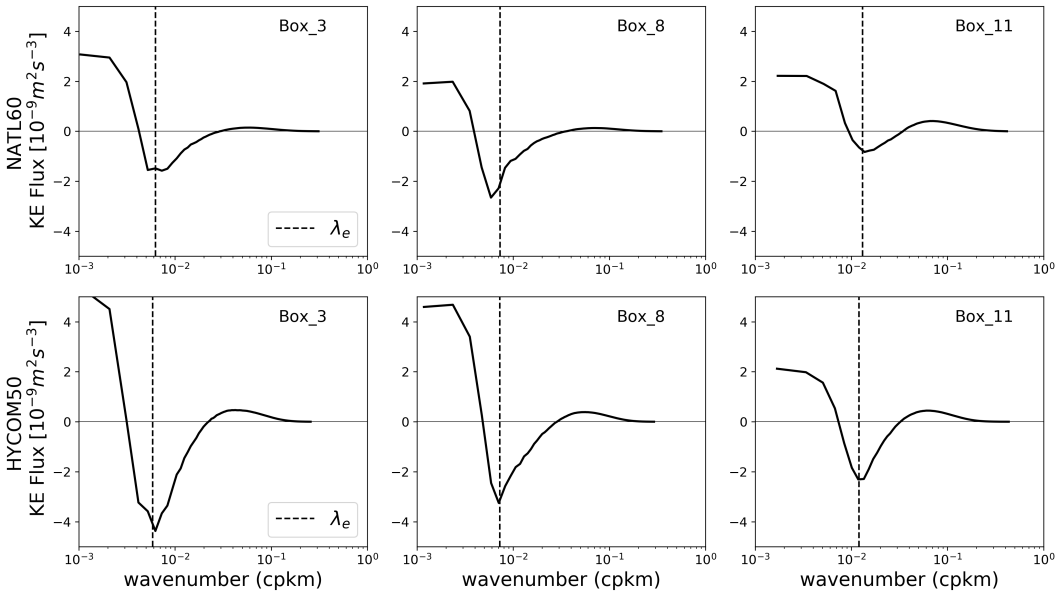

Figure 10: One year average of kinetic energy spectral flux computed from the daily output of horizontal total velocities. NATL60 (upper panel) and HYCOM50 (lower panel)

The scale at which the inverse cascade is most intense coincides with the energy-containing scale (dashed line in Figure 10) estimated from the kinetic energy spectrum. This signifies that the strength of the inverse cascade is maximum at the scale of the most energetic eddies. Just like the energy-containing scale, the scale of the most intense inverse cascade also varies with latitude with relatively smaller values in the sub-polar regions.

Figure 11 presents the KE spectral flux for Box 8 as a function depth. The overall shape of the flux is preserved and the scale at which the inverse cascade is maximum is also consistent with depth. However, the strength of inverse cascade decreases with depth and the direct cascade at high wavenumbers is confined mostly to the surface. We saw in section 1, that fine-scale structures are less energetic at depth, a consequence of that is the absence of a direct cascade of energy (at high wavenumber) at depth. The depth averaged flux for the two simulations is presented in Figure 14a.

In section 3.1, the question was raised as to whether HYCOM50's higher KE when compared to NATL60 is a consequence of HYCOM50's coarser vertical resolution which could lead to a surface intensified inverse cascade and hence more energetic surface eddies. However, in Figure 11, we can see that both at the surface and at all depth levels, the estimated inverse and direct cascade is stronger in HYCOM50 than in NATL60. This clearly indicates that HYCOM50 upscale energy flux is not surfaced intensified and we can conclude that the disparity between the two model in terms of energy levels is most likely due to differences in the length of the spin-up and

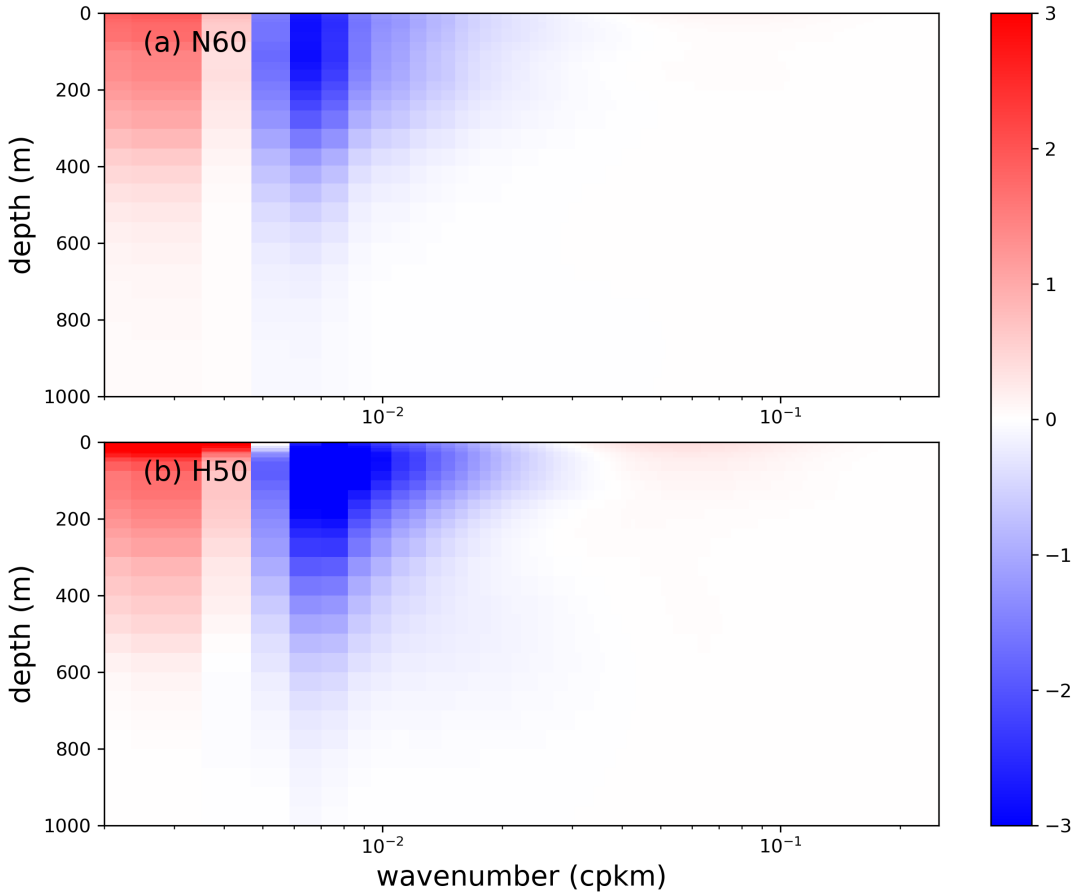

Figure 11: One year average of kinetic energy spectral flux for Box 8 computed from horizontal total velocity as a function of depth for (a) NATL60 and (b) HYCOM50. The dashed line (λ_e) is the energy containing scale estimated for the kinetic energy wavenumber spectra.

that having only 32 isopycnal vertical levels is not detrimental to the representation of the dynamics in the ocean interior.

4.1 Seasonality of energy cascade

In this section, we present the seasonality of the kinetic energy spectral flux by comparing winter (JFM) and summer (JAS) averages. Figure 12 shows the winter cascade in blue and the summer cascade in red. There are two notable differences between the seasons. First, there is a shift in the zero crossings to higher wavenumbers in winter. As previously highlighted in the preceding section, a zero-crossing at the very high wavenumbers partly indicates how much of submesoscales motions are involved in feeding large scales motions via an inverse cascade of energy. So, a shift to higher wavenumbers in wintertime signifies that smaller-scale structures are involved in fluxing energy to larger scales. Second, there is a stronger forward cascade within submesoscale wavenumber range towards dissipation in winter. Recent studies have shown that submesoscales motions are more energetic in wintertime (Sasaki et al., 2017; Rocha et al., 2016; Brannigan et al., 2015; Capet et al., 2008b) and their emergence is forced by mechanisms such as frontogenesis, wind-induced frontal instabilities, mixed layer instability among many others (Thomas, 2008; McWilliams, 2016). A possible explanation for this seasonality is that energetic submesoscale motions inject energy at small scales and part of this energy feeds larger scale motion via inverse cascade. This seasonality highlights how submesoscales motions modulate the redistribution of energy between scales of motions. Hence, the need for climate (ocean) models with submesoscale resolving capability. The seasonal differences that we see at the surface extend to the interior as well (Figure 13). The forward cascade at high wavenumbers in winter is confined within the mixed-layer depth and this corroborates what we expect, because we know that submesoscales emerging from mixed layer instability are confined to the mixed layer depth. The mean over all the depth levels is presented in Figure 14b.

It is noteworthy that the integral scale and scale of the maximum inverse cascade also undergo seasonality. There is a shift in the scale to high wavenumber from winter to summer. This can be interpreted as a reduction in the averaged size of energetic eddies structures in winter and this is consistent with the findings of Ajayi et al. (2019).

4.2 Impact of ageostrophic flows on KE flux

We have discussed so far the KE spectral flux computed using the daily output of total horizontal velocities. As mentioned earlier, NATL60 and HYCOM50 are

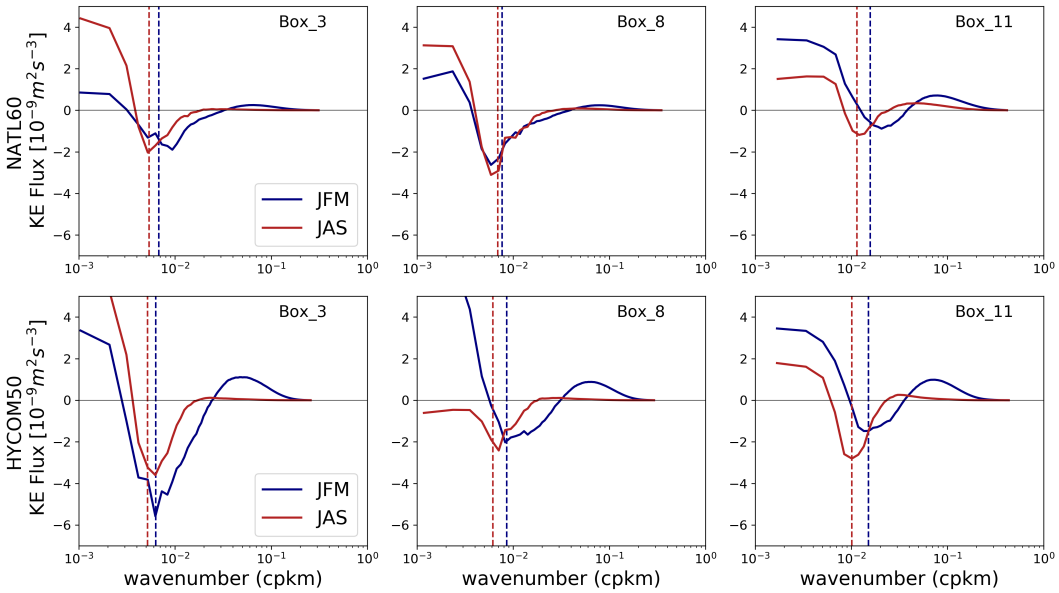

Figure 12: Winter (blue line) and summer (red line) average of kinetic energy spectral flux computed from daily output of horizontal total velocities. Dash lines represents the energy containing scale. NATL60 (upper panel) and HYCOM50 (lower panel)

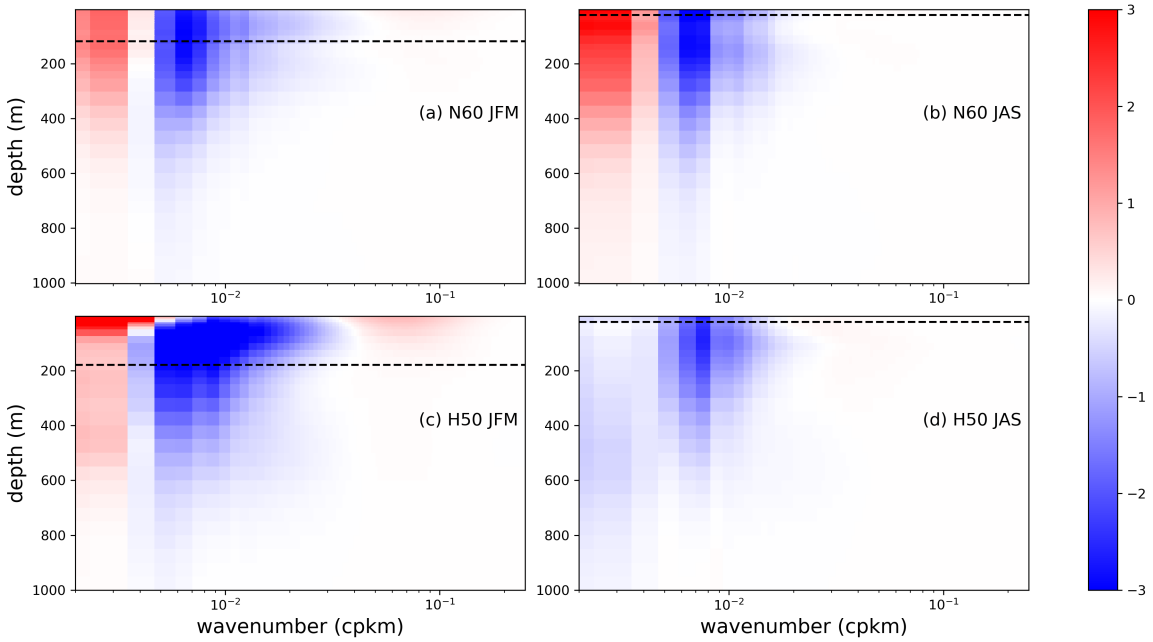

Figure 13: Winter and summer averages of kinetic energy spectral flux for Box 8 computed from horizontal total velocity as a function of depth for (a) NATL60 and (b) HYCOM50. Black dash line represents the average mixed layer depth.

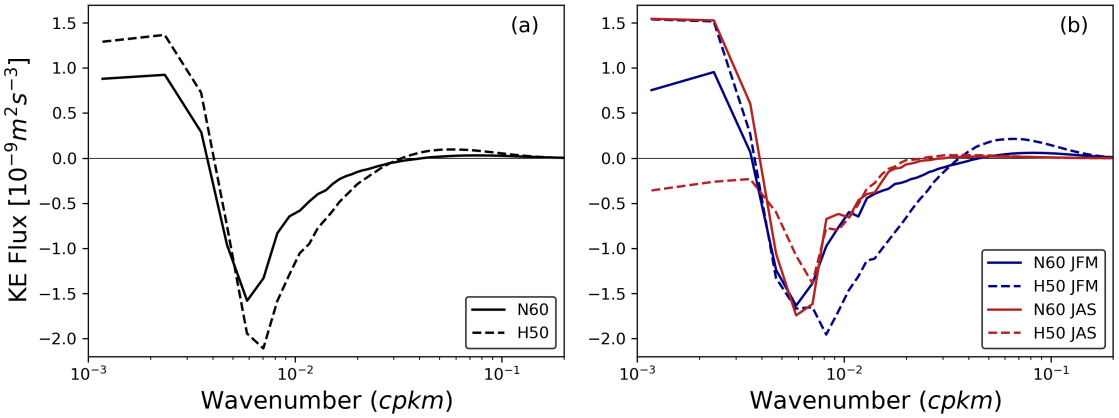

Figure 14: Kinetic energy spectra flux (averaged over 1000m depth) for Box 8 computed from daily output of horizontal total velocity for NATL60 (thick line) and HYCOM50 (dash line). (a) one year mean (b) winter (blue line) and summer (red line) averages.

submesoscale permitting model simulations that have been created to simulate the scales of motions that we expect SWOT to see from space. SWOT like every other satellite mission will provide the measurement of sea surface heights from which velocities (based on geostrophic approximations) are inferred. The world ocean is predominantly dominated by geostrophically balanced motions at meso and large scale, and the inferred geostrophic velocities at this scale mostly reflect the absolute velocity of these large scales motions. However, geostrophy is less accurate for fine-scale motions and this questions our ability to trust satellite altimeter to resolve effectively the energetics of fine-scale motions in terms of energy redistribution within the submesoscales range (<50 km). SWOT will provide information down to 15km and we are curious to see if the geostrophically inferred surface velocity would capture the true energetics at scales less than 50 km where geostrophy is likely to fail.

In Figure 15, we present the spectral flux from total velocity and geostrophic velocity for three regions (same as for the previous sections). The strength of the energy cascade differs between the flux computed from the total velocity and that of the geostrophic velocity. This difference is consistent in all the three boxes and in the two models. In particular, at the very high wavenumbers, the strength of the forward cascade is underestimated in the flux computed from the geostrophic velocity. A possible reason for this mismatch at smaller scales could be explained by findings of Brüggemann and Eden (2015) that showed that ageostrophic flows at fine scales are a good catalyst for energy cascade towards dissipation. Despite the differences in terms of flux magnitude, the overall shape of the flux is consistent for the two forms of spectral flux. In fact, the scale of the maximum inverse cascade is the same irrespective of the type of velocity fields.

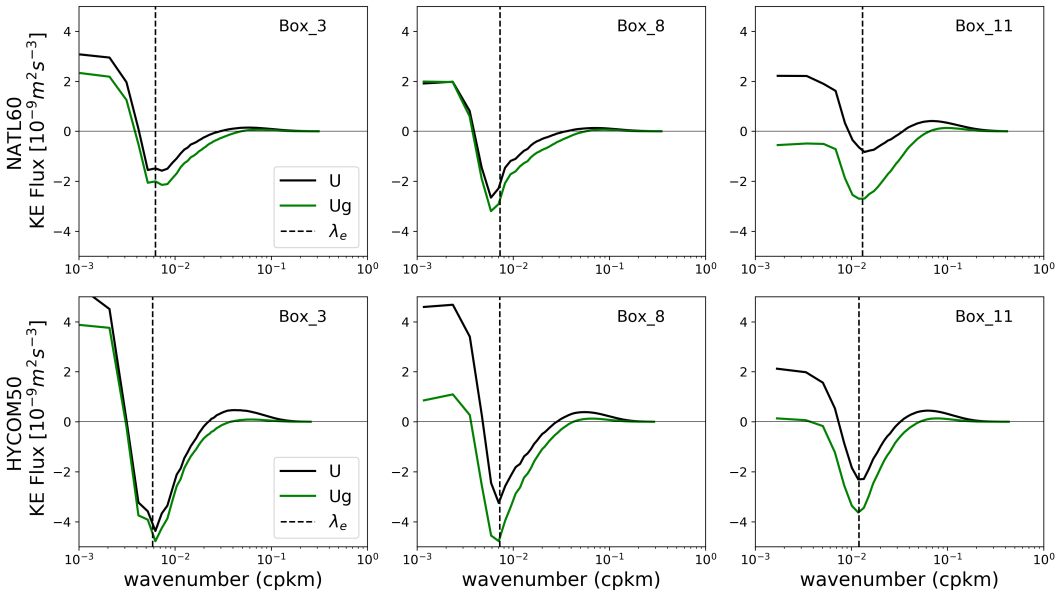

Figure 15: Kinetic energy spectral flux computed from total velocity (black line) versus spectral flux computed from geostrophic velocity (green line). NATL60 (upper panel) and HYCOM50 (lower panel)

5 Discussion and Summary

Kinetic energy wavenumber spectra density, slope, and flux are estimated in this study. The analysis presented has shown that the North Atlantic ocean follows the framework of quasi-geostrophy dynamic with a KE spectral shape of $\sim k^{-3}$ almost everywhere. Owing to the ability of our kilometric ocean models (NATL60 and HYCOM50) to reasonably resolve fine-scale structures down to 10km, kinetic energy spectral flux computed from daily outputs of horizontal total velocities revealed an overall net inverse cascade of energy with a significant direct cascade of energy at high wavenumbers. The cascade as a function of depth reveal that the forward cascade at high wavenumber is confined to the mixed layer depth while the inverse cascade dominates the water column down to 700m. We showed that the maximum inverse cascade occurs at a scale that coincides with the energy-containing scale estimated from the kinetic energy wavenumber spectra.

The results presented in this study are based on the analysis of two kilometric simulations outputs with similar horizontal grid space but different numerics, sub-grid parametrization and vertical resolution. In particular, NATL60 has 300 z levels while HYCOM50 has 32 hybrid layers. Despite these differences, the two simulations agree well on the overall dynamics of the North Atlantic. Having said that, HYCOM50 show stronger energy level compared to NATL60 both at the surface and in the interior. We found the estimated cascade in HYCOM50 to be of higher magnitude compared to NATL60 for both direct and inverse cascade. The difference

in energetics between the two models is possibly due to the difference in the length of the spin-up or the subgrid scale parameterization choices. Initially, we thought that HYCOM50 having just 32 hybrid layers in the vertical could lead to a more surface intensified energy cascade in HYCOM50 than in NATL60. But this is not the case, because across all scales and at depth, HYCOM50 seems to show stronger energetics compared to NATL60.

NATL60 and HYCOM50 are designed particularly to serve as an observational dataset for the much-anticipated SWOT mission. So what is the implication of our results for the upcoming fine-scale resolving satellite mission SWOT? From SWOT we will able get surface geostrophic velocity as usual hence we can compute cross-scale energy transfer. Our results show that not accounting for ageostrophic fine-scale motions underestimates the forward cascade of energy.

References

Ajayi, A., Le Sommer, J., Chassignet, E., Molines, J.M., Xu, X., Albert, A., Cosme, E., 2019. Spatial and Temporal Variability of North Atlantic Eddy Field at Scale less than 100km. In preparation for Journal of Ocean Modelling .

Aluie, H., Hecht, M., Vallis, G.K., 2017. Mapping the Energy Cascade in the North Atlantic Ocean: The Coarse-graining Approach. J. Phys. Oceanogr. , 225–244doi:10.1175/JPO-D-17-0100.1.

Amores, A., Jorda, G., Arsouze, T., Le Sommer, J., 2018. Up to What Extent Can We Characterize Ocean Eddies Using Present-Day Gridded Altimetric Products? Journal of Geophysical Research: Oceans 123.

Brannigan, L., Marshall, D.P., Naveira-Garabato, A., George Nurser, A.J., 2015. The seasonal cycle of submesoscale flows. Ocean Modelling .

Brüggemann, N., Eden, C., 2015. Routes to Dissipation under Different Dynamical Conditions. J. Phys. Oceanogr. 45, 2149–2168. doi:10.1175/JPO-D-14-0205.1.

Callies, J., Ferrari, R., Klymak, J.M., Gula, J., 2015. Seasonality in submesoscale turbulence. Nature Communication 6, 6862.

Capet, X., Campos, E.J., Paiva, A.M., 2008a. Submesoscale activity over the Argentinian shelf. Geophysical Research Letters 35, 2 – 6.

Capet, X., Mcwilliams, J.C., Molemaker, M.J., Shchepetkin, A.F., 2008b. Mesoscale to Submesoscale Transition in the California Current System. Part I: Flow Structure, Eddy Flux, and Observational Tests. J. Phys. Oceanogr. 38, 29 – 43. doi:10.1175/2007JPO3671.1.

Charney, J., 1971. Geostrophic turbulence. Journal of Atmospheric Sciences 28, 1087–1095.

Chassignet, E.P., Xu, X., 2017. Impact of Horizontal Resolution (1/12 to 1/50) on Gulf Stream Separation, Penetration, and Variability. Journal of Physical Oceanography 47, 1999 – 2021.

Ducousso, N., Le Sommer, J., Molines, J.M., Bell, M., 2017. Impact of the symmetric instability of the computational kind at mesoscale- and submesoscale-permitting resolutions. Ocean Modelling 120.

Dufau, C., Orsztynowicz, M., G., D., R., M., P.Y., L.T., 2016. Mesoscale resolution capability of altimetry: Present and future. J. Geophys. Res. Oceans 121, 1–18. doi:10.1175/JPO-D-11-0240.1.

Dussin, R., Barnier, B., Brodeau, L., Molines, J.M., 2018. The making of the DRAKKAR forcing set DFS5. Drakker .

Eden, C., 2007. Eddy length scales in the North Atlantic Ocean. Journal of Geophysical Research 112, C06004.

Ferrari, R., Wunsch, C., 2009. Ocean Circulation Kinetic Energy: Reservoirs, Sources, and Sinks. Annu. Rev. Fluid Mech. 41, 253–282. doi:10.1146/annurev.fluid.40.111406.102139.

Fresnay, S., Ponte, A.L., Le Gentil, S., Le Sommer, J., 2018. Reconstruction of the 3-D Dynamics From Surface Variables ina High-Resolution Simulation of North Atlantic. Journal of Geophysical Research: Oceans 123.

Fu, L.L., Chelton, D.B., Le Traon, P.Y., Morrow, R., 2010. Eddy Dynamics From Satellite Altimetry. Oceanography 23, 14–25.

Fu, L.L., Ferrari, R., 2008. Observing oceanic submesoscale processes from space. Eos, Transactions, American Geophysical Union 48, 488.

Khatri, H., Sukhatme, J., Kumar, A., Verma, M.K., 2018. Surface Ocean Enstrophy, Kinetic Energy Fluxes and Spectra from Satellite Altimetry. J. Geophys. Res. Ocean. doi:10.1029/2017JC013516.

Kjellsson, J., Zanna, L., 2017. The Impact of Horizontal Resolution on Energy Transfers in Global Ocean Models. Fluids 2, 45. doi:10.3390/fluids2030045.

Le Sommer, J., Molines, J.M., Albert, A., Brodeau, L., Ajayi, A.O., Gomez Navarro, L., Cosme, E., Penduff, T., Barnier, B., Verron, J., Brasseur, P., Rampal, P., Chassignet, E., 2019. NATL60: A North Atlantic ocean circulation model dataset based on NEMO for preparing SWOT altimeter mission, in prep. In preparation for Geoscientific Model Development. .

Le Traon, P.Y., Klein, P., Hua, B.L., Dibarboure, G., 2008. Do altimeter data agree with interior or surface quasi- geostrophic theory? Journal of Physical Oceanography 5, 1137 1142.

Le Traon, P.Y., Rouquet, M.C., Boissier, C., 1990. Spatial scales of mesoscale variability in the North Atlantic as deduced from Geosat data. Journal of Geophysical Research 95, 20267.

McWilliams, J.C., 2016. Submesoscale currents in the ocean. Proc. R. Soc. A 472, 20160117.

Oscar, V., Rosemary, M., Marie-Isabelle, P., Dibarboure, G., Clement, U., 2018. Revised Global Wave Number Spectra From Recent Altimeter Observations. Journal of Geophysical Research : Oceans .

Qiu, B., Chen, S., Klein, P., Sasaki, H., Sasai, Y., 2014. Seasonal Mesoscale and Submesoscale Eddy Variability along the North Pacific Subtropical Countercurrent. Journal of Physical Oceanography 44, 3079 – 3098.

Rocha, C.B., Gille, S.T., Chereskin, T.K., M., D., 2016. Seasonality of submesoscale dynamics in the Kuroshio Extension. Geophysical Research Letters 43, 11304 – 11311.

Salmon, R., 1980. Baroclinic instability and geostrophic turbulence. Geophys. Astrophys. Fluid Dyn. 15, 167211.

Sasaki, H., Klein, P., 2012. SSH Wavenumber Spectra in the North Pacific from a High-Resolution Realistic Simulation. J. Phys. Oceanogr. 42, 1233–1241. doi:10.1175/JPO-D-11-0180.1.

Sasaki, H., Klein, P., Qiu, B., Sasai, Y., 2014. Impact of oceanic scale- interactions on the seasonal modulation of ocean dynamics by the atmosphere. Nature Communication 5, 5636.

Sasaki, H., Klein, P., Sasai, Y., Qiu, B., 2017. Regionality and seasonality of submesoscale and mesoscale turbulence in the North Pacific Ocean. Ocean Dynamics 67, 1195 – 1216.

Scott, R.B., Arbic, B.K., 2007. Spectral Energy Fluxes in Geostrophic Turbulence: Implications for Ocean Energetics. J. Phys. Oceanogr. 37, 673–688. doi:10.1175/JPO3027.1.

Scott, R.B., Wang, F., 2005. Direct Evidence of an Oceanic Inverse Kinetic Energy Cascade from Satellite Altimetry. J. Phys. Oceanogr. 35, 1650–1666. doi:10.1175/JPO2771.1.

Smith, S., Vallis, G., 2002. The Scales and Equilibration of Mid Ocean Eddies: Forced Dissipative Flow. J. Phys. Oceanogr. 32, 1699–1720.

Soufflet, Y., Marchesiello, P., Lemari, F., Jouanno, J., Capet, X., Debreu, L., Benshila, R., 2016. On effective resolution in ocean models. Ocean Model. 98, 36–50. doi:10.1016/j.ocemod.2015.12.004.

Stammer, D., Böning, C.W., 1992. Mesoscale Variability in the Atlantic Ocean from Geosat Altimetry and WOCE High-Resolution Numerical Modeling.

Thomas, L., 2008. Submesoscale processes and dynamics. Geophysical Monograph Series 177. doi:https://doi.org/10.1029/177GM04.

Tulloch, R., John, M., Chris, H., 2011. Scales, Growth Rates, and Spectral Fluxes of Baroclinic Instability in the Ocean. J. Phys. Oceanogr. 41, 1057–1076. doi:10.1175/2011JPO4404.1.

Uchida, T., Abernathey, R., Smith, S., 2017. Seasonality of eddy kinetic energy in an eddy permitting global climate model. Ocean Modelling 118, 41 – 58.

Uppala, S.M., Kållberg, P.W., Simmons, A.J., Andrae, U., da Costa Bechtold, V., Fiorino, M., Gibson, J.K., Haseler, J., Hernandez, A., Kelly, G.A., Li, X., Onogi, K., Saarinen, S., Sokka, N., Allan, R.P., Andersson, E., Arpe, K., Balmaseda, M.A., Beljaars, A.C., van de Berg, L., Bidlot, J., Bormann, N., Caires, S., Chevallier, F., Dethof, A., Dragosavac, M., Fisher, M., Fuentes, M., Hagemann, S., Hólm, E., Hoskins, B.J., Isaksen, L., Janssen, P.A., Jenne, R., McNally, A.P., Mahfouf, J.F., Morcrette, J.J., Rayner, N.A., Saunders, R.W., Simon, P., Sterl, A., Trenberth, K.E., Untch, A., Vasiljevic, D., Viterbo, P., Woollen, J., 2005. The ERA-40 re-analysis. Q. J. R. Meteorol. Soc. 131, 2961–3012. doi:10.1256/qj.04.176.